Glycoconj J (2013) 30:747–757
DOI 10.1007/s10719-013-9478-6

Influence of ligand presentation density on the molecular recognition of mannose-functionalised glyconanoparticles by bacterial lectin BC2L-A

Michael Reynolds · Marco Marradi · Anne Imberty · Soledad Penadés · Serge Pérez

Received: 25 March 2013 / Accepted: 24 April 2013 / Published online: 11 May 2013
© Springer Science+Business Media New York 2013

Abstract Polyvalent carbohydrate-protein interactions play a key role in bio- and pathological processes, including cell-cell communication and pathogen invasion. In order to study, control and manipulate these interactions gold nanoparticles have been employed as a 3D scaffold, presenting carbohydrate ligands in a multivalent fashion for use as high affinity binding partners and a model system for oligosaccharide presentation at biomacromolecular surfaces. In this study, the binding of a series of mannose-functionalised gold nanoparticles to the dimeric BC2L-A lectin from *Burkholderia cenocepacia* has been evaluated. BC2L-A is known to exhibit a high specificity for (oligo)mannosides. Due to the unique structure and binding nature of this lectin, it provides a useful tool to study (oligo)saccharides presented on multivalent scaffolds. Surface plasmon resonance and isothermal titration calorimetric assays were used to investigate the effect of ligand presentation density towards binding to the bacterial lectin. We show how a combination of structural complementarities between ligand presentation and lectin architecture and statistical re-binding effects are important for increasing the avidity of multivalent ligands for recognition by their protein receptors; further demonstrating the application of glyconanotechnology towards fundamental glycobiology research as well as a potential towards biomedical diagnostics and therapeutic treatments.

Keywords Lectin · Multivalency · Glyconanoparticles · Protein-carbohydrate interaction

Introduction

Specific, reversible carbohydrate recognition by protein receptors, lectins, has long been implicated in many normal and pathological processes from cell recognition and communication to pathogen invasion and tumour metastasis [1, 2]. Despite the high specificity of lectins towards their carbohydrate ligands, these interactions typically exhibit relatively weak affinities. To compensate for this, lectins often form multimeric architectures presenting several binding sites. Similarly, the carbohydrate ligands are often presented multivalently or as clusters; the overall interaction thus being a combination of several binding events, resulting in significantly higher affinity. This multivalence effect has been attributed to statistical effects such as effective concentrations and rebinding phenomena, as well as specific structural complementarities between ligand and

Electronic supplementary material The online version of this article (doi:10.1007/s10719-013-9478-6) contains supplementary material, which is available to authorized users.

M. Reynolds · A. Imberty · S. Pérez (✉)
Centre de Recherche sur les Macromolécules Végétales (CERMAV – CNRS), affiliated with Université Joseph Fourier Grenoble and ICMG, BP 53, 38041 Grenoble, France
e-mail: spsergeperez@gmail.com

M. Reynolds
European Synchrotron Radiation Facility, 6 Rue Jules Horowitz, BP 220, 38043 Grenoble cedex 9, France

M. Marradi · S. Penadés
Biofunctional Nanomaterials Unit, Biomedical Research Networking Center in Bioengineering, Biomaterials and Nanomedicine (CIBER-BBN),
Pº Miramón 182, 20009 San Sebastian, Spain

receptor presentations, or indeed, a combination of all of these [3–6].

Over the last decade, efforts were made towards the construction of well defined platforms for presenting carbohydrates in order to study, control or inhibit multivalent lectin-carbohydrate interactions. As a result of this, several multivalent glycoconjugates based on different molecular scaffolds have been designed and prepared to enhance the affinity of carbohydrate ligands towards their protein receptors, to target pathogen activity in particular [7]. As part of this approach, Glyco-nanoparticles (GNPs) [8] *i.e.* exceptionally small gold nanoparticles with a self-assembled monolayer of carbohydrate ligands at their surface, have been produced with varying ligand valencies and presentation densities [8–10]. Their synthesis, potentially with several different ligands in variable densities, can be made in one step which allows for tuning physico-chemical properties. This in turn offers the opportunity for GNPs with multiple functionalities and interesting diagnostic opportunities ("smart" drug delivery agents, fluorescence imaging, magnetism, SERS, *etc.*) [11]. Several examples of the use of GNPs towards protein-carbohydrate interactions can be found in the literature [12–20]. We have recently used galactose-functionalised GNPs to characterise their recognition by the LecA/PA-IL lectin from *Pseudomonas aeruginosa* [21].

Burkholderia cenocepacia is an opportunistic bacterial pathogen responsible for numerous nosocomial infections which primarily affects, with significant mortality, cystic fibrosis patients and the immuno compromised [22]. Infections with *B. cenocepacia* are also implied in co-infection with *Pseudomonas aeruginosa* and exhibit intrinsic antiobiotic resistance [23]. As part of the pathogen invasion process, it is suspected that the bacteria use soluble lectins to bind to glycoconjugates present on epithelial cells and mucus of the host [24]. Several of these lectins have been identified within the bacteria, isolated and characterised for their carbohydrate specificities [24–26]. The smallest of which, *Burkholderia cenocepacia* lectin A, BC2L-A, is a member of the LecB/PA-IIL lectin family (from *Pseudomonas aeruginosa*) with a core β-sheet structure and a dependence on two Ca^{2+} ions for binding, but is novel in that it only associates as a homo-dimer, demonstrates site co-operativity and exhibits a high specificity for mannose and mannose oligosaccharides [27]. Due to the lectin's unique structure, binding characteristics, binding affinity (K_d for Me-α-D-Man~3 μM, compared to 120 μM for ConA) [24, 28], and efficient recombinant expression protocol it provides a potential as both an interesting target for anti-adhesive therapy for preventing *B. cepacia* invasion, and a useful tool to study multivalent scaffolds developed to investigate protein-carbohydrate interactions. Rieger *et al.* had previously used BC2L-A (referred to as BclA in their articles) to study the availability of mannose residues on functionalised polymer micelles and nanoparticles [29, 30]. Di- and trisaccharides, as well as small dimeric molecules, were also used to further probe the lectin binding site [27].

Here we use mannose-functionalised GNPs to study and characterise their multivalent molecular recognition by the BC2L-A lectin, using surface plasmon resonance and isothermal titration calorimetry techniques. We show that mannose avidity is dependent on presentation density at the GNP surface, with the most effective GNP exhibiting a K_d of 19 nM per monosaccharide ligand, the most effective ligand of BC2L-A to date. Furthermore, by combining typical AuNP characterisation techniques with quantitative interaction studies and the unique binding properties of this lectin, we were able to probe ligand presentation at GNP surfaces.

Material and methods

General procedures All starting materials were purchased from Sigma-Aldrich and used without further purification with the exception of tetrachloroauric acid which was purchased from Strem Chemicals and used without further purification. Laboratory distilled water was further purified using a Milli-Q water purification system. GNP preparation and characterisation was documented in our previous study [21]. For consistency, the labelling of synthesised molecules and GNPs has been kept in the same format.

Small angle X-ray scattering Aqueous nanoparticle solutions of 2 mg mL^{-1} were prepared and centrifuged for 2×5 min at 13,000 rpm. SAXS was carried out at the ID02 high brilliance and ID13 microfocus beamlines of the European Synchrotron Radiation Facililty (ESRF) using a monochromatic beam of λ=1.0597 Å (E=11.7 keV) and λ=1 Å (E=12.39 keV) respectively. Sample-detector distances of 1.5 m and 0.787 m were used giving q ranges of 0.06–4 and 0.2–3 nm^{-1} respectively. SAXS patterns were recorded by a 16 bit readout FReLoN charge coupled device (CCD) detector with 2,048×2,048 pixels of 51×51 μm^2 binned to 512×512 pixels. Nanoparticle and water solutions were studied in a 1.7 mm diameter flow-through cell or 200 μm glass capillary. SAXS patterns were obtained after correction and background subtraction. Between 5 and 10 SAXS patterns were corrected and averaged for fitting. Data analysis was carried out using the *SAXSutilities* package (www.sztucki.de/SAXSutilities) [31]. A core-shell model from this package was used to fit the SAXS patterns. Core radii and polydispersity were set to those taken from TEM. Shell radii were extracted from the fits.

Recombinant proteins The lectin BC2L-A, from *Burkholderia cenocepacia* was expressed and purified in recombinant form from *Escherichia coli* as documented previously [24].

Surface plasmon resonance assays All SPR experiments were carried out on a Biacore T100 instrument. CM5 sensor chips (Biacore/GE, Uppsala, Sweden) were equilibrated with HBS (HEPES-buffered saline: 10 mm HEPES and 150 mm NaCl, pH 7.4) containing 0.005 % (v/v) Tween 20 at 25 °C with a flow rate of 20 μL min^{-1}. Following equilibration, the chips were activated with two 7 min pulses of a 1 : 1 mixture (v/v) of 0.1 M *N*-hydroxy-succinimide and 0.1 M *N*-ethyl-*N*′-(dimethylaminopropyl)carbodiimide, at 25 °C and flow rate of 5 μL min^{-1}. Ethanolamine hydrochloride was immobilised on channel 1 *via* an injection of 7 min (1.0 M, pH 8.5; ~80 RU) to measure the level of non-specific binding and to serve as a blank for mathematical data treatment. BC2L-A was immobilised to channel 2 *via* an injection of 7 min (10 μg mL^{-1}, sodium acetate buffer, pH 4.5; ~480 RU). Remaining *N*-hydroxy succinimide esters were blocked by a 7 min pulse of 1 M ethanolamine hydrochloride, pH 8.5. PA-IL was immobilised to Channel 3 *via* an injection of 41 mins (100 μg mL^{-1}, sodium acetate buffer, pH 4.5; ~300 RU). Remaining *N*-hydroxy succinimide esters were blocked by a 7 min pulse of 1 M ethanolamine hydrochloride, pH 8.5.

Affinity measurements GNP solutions (2 μg mL^{-1}, and dilutions thereof to 30 ng mL^{-1}) in HEPES buffer were flowed across the sensor chip surfaces for 3 min at a flow rate of 20 μL min^{-1}, and were allowed to dissociate for 3 min. To regenerate the surfaces, injections of three 3×3 min pulses of 100 mM Me-α-D-mannoside were performed. A repeat injection of a sample solution at 125 ng mL^{-1} concentration was used to confirm surface regeneration at the end of the concentration series. Binding was measured as RU (resonance units) over time. Affinity (k_a) and dissociation (k_d) rate constants were calculated using the BIA evaluation software 1.1 (Biacore). Curves were fitted to a single 1:1 binding model, which gave the best fit as judged by the lowest χ^2 value and the best distribution of residuals. Association constants (K_a) were calculated from the equation: $K_a = 1/K_d = k_a/k_d$.

Microcalorimetry All solutions were centrifuged at 13 krpm for 2×5 min at 4 °C. Titration calorimetry experiments were performed using a Microcal VP-ITC microcalorimeter. Titrations were carried out in 0.1 M Tris/HCl buffer (pH 7.5) containing 3 μm $CaCl_2$, at 25 °C. 30 aliquots of 10 μL of BC2L-A solution (concentrations of 0.21 mM to 1 mM) were added at 5 min intervals to the GNP solution present in the calorimeter cell. The GNP concentration varied from 0.5 mg mL^{-1} to 1.73 mg mL^{-1}, giving a saccharide concentration of 0.013 mM to 0.160 mM. The corresponding molecule **3** was also injected into solutions of BC2L-A. Concentrations of **3** were 3 mM and BC2L-A concentrations 0.31 mM. The temperature of the cell was controlled to 25±0.1 °C. Control experiments performed by

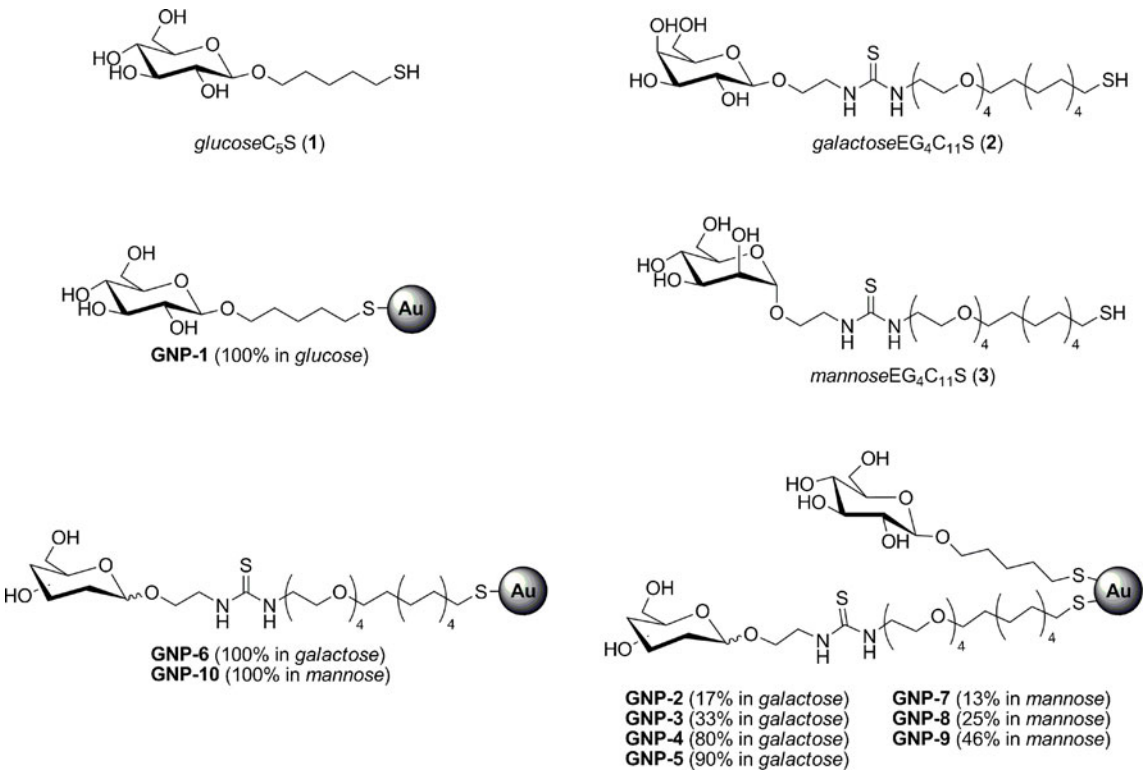

Fig. 1 Ligands **1** – **3** synthesised for protecting Au clusters **GNP-1** – **GNP-10**. For clarity neoglycoconjugates **1** – **3** are depicted as thiols, although they were isolated as a mixture of thiol and disulfide

Table 1 Summary of GNPs synthesised

GNP	Average core diameter (nm)	Shell thickness (nm)	Average no. of Au atoms[a]	Average molecular formula	Average GNP valency (%)	Average GNP valency	Average M_w[a] (kDa)	Average inter-ligand distance, s[b] (nm)
Glc								
GNP-1	(1.3±0.3)	0.9	100	$(C_{11}H_{21}O_6S)_{41}Au_{100}$	0	0	31.2	–
Gal/Glc					*Galactose*-Valency			
GNP-2	(1.4±0.5)	1.9	120	$(C_{28}H_{55}N_2O_{10}S_2)_{12}(C_{11}H_{21}O_6S)_{59}Au_{120}$	12	17	47.9	(2.9±0.4)
GNP-3	(1.3±0.3)	2.2	79	$(C_{28}H_{55}N_2O_{10}S_2)_{15}(C_{11}H_{21}O_6S)_{30}Au_{79}$	15	33	33.6	(2.8±0.3)
GNP-4	(1.4±0.3)	–	140	$(C_{28}H_{55}N_2O_{10}S_2)_{65}(C_{11}H_{21}O_6S)_{16}Au_{140}$	65	80	73.9	(1.6±0.2)[c]
GNP-5	(1.4±0.3)	–	100	$(C_{28}H_{55}N_2O_{10}S_2)_{57}(C_{11}H_{21}O_6S)_7Au_{100}$	57	90	58.3	(1.7±0.2)[c]
GNP-6	(1.2±0.3)	2.6	70	$(C_{28}H_{55}N_2O_{10}S_2)_{67}Au_{70}$	67	100	56.9	(1.6±0.1)
Man/Glc					*Mannose*-Valency			
GNP-7	(1.5±0.4)	1.7	125	$(C_{28}H_{55}N_2O_{10}S_2)_{11}(C_{11}H_{21}O_6S)_{72}Au_{125}$	11	13	51.9	(2.9±0.6)
GNP-8	(1.7±0.4)	2.2	140	$(C_{28}H_{55}N_2O_{10}S_2)_{24}(C_{11}H_{21}O_6S)_{72}Au_{140}$	24	25	63.3	(2.4±0.2)
GNP-9	(1.6±0.4)	2.7	140	$(C_{28}H_{55}N_2O_{10}S_2)_{39}(C_{11}H_{21}O_6S)_{46}Au_{140}$	39	46	65.6	(2.2±0.3)
GNP-10	(1.4±0.4)	2.6	116	$(C_{28}H_{55}N_2O_{10}S_2)_{88}Au_{116}$	88	100	79.5	(1.4±0.1)

[a] The average number of gold atoms in the cluster, the molecular formulae, and the molecular weights were calculated according to the average gold core diameter by TEM and elemental analysis [32]

[b] Errors are the variation in valency for the population of nanoparticles

[c] Shell thickness extrapolated from the shell thickness model

injection of buffer into the GNP solution yielded insignificant heats of dilution. Injections of lectin into control (galactose-functionalised) GNPs yielded heats of dilution, which were subtracted from experimental data during the data processing phase. Integrated heat effects were analysed by non-linear regression using a two-site binding model (Origin 7.0, OriginLab Corp.). Fitted data yielded association constants (K_a) and the enthalpy of binding (ΔH). Other thermodynamic parameters, *i.e.* changes in free energy, ΔG, and entropy, ΔS, were calculated from the equation: $\Delta G = \Delta H - T\Delta S = -RT \ln K_a$ where T is the absolute temperature and R=8.314 J mol^{-1} K^{-1}. Two to three independent titrations were performed for each lectin — GNP combination.

Results and discussion

Synthesis

Hybrid *mannose*-, *galactose*- and *glucose*-GNPs displaying different ligand presentation densities were prepared as in previous studies (Fig. 1 and Table 1) [17, 21]. For consistency, the labelling of synthesised GNPs has been kept in the same format as our previous work with PA-IL [21]. The thiol-functionalised glucose neoglycoconjugate **1** has a short five carbon linear aliphatic chain and acts as an inert ligand with respect to BC2L-A recognition. Mannose neoglycoconjugate **3** exhibits a thiol-functionalised amphiphilic linker which imparts good chemisorption to the Au cluster whilst allowing water solubility and ligand flexibility. The 100 % mannose-functionalised glyconanoparticles (**GNP-10**) exhibit high ligand valency and ligand presentation densities whereas mannose/glucose hybrids **GNP-7** – **GNP-9** were prepared using different ratios of neoglycoconjugates **1** and **3** in order to study the influence of mannose presentation density on molecular recognition by BC2L-A. Glucose-**GNP-1** and galactose/glucose hybrids **GNP-2** – **GNP-6** were prepared as negative controls for the assays. GNPs were characterised by ^{1}H NMR, FT-infrared spectroscopy, UV–vis spectroscopy, elemental analysis, transmission electron microscopy (TEM) and small angle X-ray scattering (SAXS) as previously reported [21]. The average number of mannosides per GNP were calculated from elemental analysis and gold cluster size (1.2–1.7 nm in diameter as determined by TEM, Table 1). For ITC experiments, absolute mannoside concentrations were also measured using the PhOH-H_2SO_4 method as previously described [21]. SAXS data were acquired in aqueous solution and analysed using the *SAXSutilities* package (www.sztucki.de/SAXSutilities) [31]. A core-shell model was used to fit the SAXS data, with core radii and core distribution restricted to those measured by TEM. From these data, the shell thickness was estimated for each GNP ligand coverage. All GNPs proved stable and soluble in aqueous environments with the exception

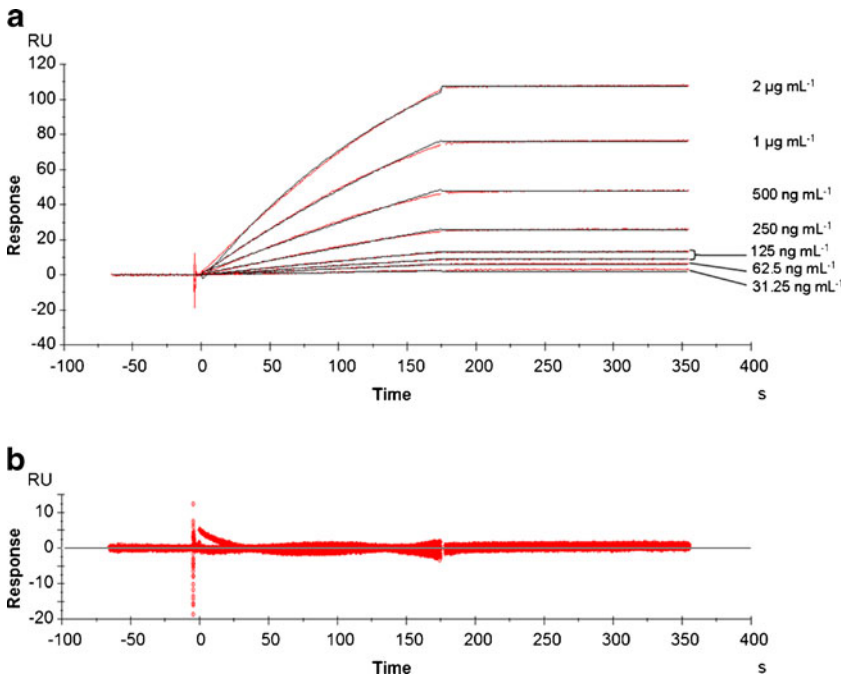

Fig. 2 **a** SPR sensorgram for solutions of GNP-9 passing over a CM5 channel functionalised with 500 RUs of BC2L-A. GNP serial dilutions of 2 µg mL^{-1} to 31.25 ng mL^{-1} were made. **b** Plots showing deviations of data points from the fit (residuals) are also shown. *Red points* represent the data points, the *black lines* represent the theoretical fits

of **GNP-10** which were not soluble in sufficient quantity in buffer solutions for ITC measurements.

Although considerable advances have recently been made with regard to the elucidation of the structure of gold clusters [33–36], there is still a significant amount of information to be gained with respect to ligand conformation and cluster behaviour, and how ligands bind to the particle surface. By combining the results of TEM and solution phase SAXS with a mathematical model adapted from Hill *et al.* [37] and Cederquist *et al.* [38] ligand display and inter-ligand distance at the nanoparticle surface can be described. In order to do this however, we assume that the Au clusters are spherical in shape, their size and size distributions correspond to those measured by TEM, absolute GNP valency corresponds to the "average" GNP and ligands are distributed uniformly around the Au cluster (see Supporting Information for details). The shell thicknesses and calculated inter-ligand distances for the GNPs are given in Table 1.

It was found that GNP shell thickness varied with ligand presentation density. The length of a free "active" ligand molecule (**2** or **3**, thiol form), not attached to a nanoparticle surface, was measured as 3.6 nm after energy minimisation in vacuum, calculated using the SYBYL graphics package (Tripos Associates, St. Louis, MO). At a 100 % presentation density of active ligands **2** or **3** (**GNP-6** and **GNP-10**), the shell thickness was found to be only 2.6 nm (Table 1). This implies that the active ligands are not presented linearly normal to the Au surface (for nanoparticles of this size and radius of curvature). Indeed, self-assembled monolayers of aliphatic chains on gold surfaces may be tilted relative to the surface normal [39]. Furthermore, ethylene glycols are known to be very flexible in aqueous solution. Therefore we suppose the hydrophilic TEG moieties will have high degrees of freedom at the GNP surface maximising non-covalent contacts with other surface bound molecules and solvent. As the presentation density decreases, the shell thickness shrinks to 1.9 nm and 1.7 nm for **GNP-2** and **GNP-7**, respectively. This would mean the active ligands are less tightly packed at the Au surface and the ethylene glycol moieties would experience less steric contacts.

Table 2 Affinity and dissociation rate constants and calculated Ka and Kd as measured for BC2L-A by SPR. Data shown are based on single measurements

GNP	k_a (10^3 M^{-1} s^{-1})	k_d (10^{-6} s^{-1})	K_a (10^9 M^{-1})	K_d (nM)
GNP-7	79	342	0.23	4.33
GNP-8	175	55	3.16	0.32
GNP-9	233	0.1	2 270	0.000 4
GNP-10	855	58	14.74	0.07

Following typical chemical characterisation of the GNPs described above, ligand presentation at GNP surfaces was further investigated by studying their recognition by the BC2L-A lectin receptor. In order to do this in a quantitative manner, the kinetics and thermodynamics of the lectin/GNP interaction were measured using surface plasmon resonance (SPR) and isothermal titration calorimetry (ITC), respectively.

Surface plasmon resonance binding assays

SPR was performed on a Biacore T100 (Biacore/GE Uppsala, Sweden) with 500 RUs of BC2L-A immobilised to a CM5 chip *via* NHS-EDC coupling kit. Ethanolamine was also immobilised to a second channel of the CM5 sensor chip to

serve as a blank surface. A third channel was functionalised with 300 RUs of the galactose-specific lectin PA-IL as a negative control for non-specific *mannose*-GNP interactions and a positive control for *galactose*-GNP activity. Solutions of **GNP-1** – **GNP-10** in HEPES buffer were flowed over the sensor chip with concentrations of 2 μg mL^{-1} and dilutions thereof to 30 ng mL^{-1}. As expected the mannose-functionalised **GNP-7** – **GNP-10** showed significant binding to the BC2L-A surface (see Supporting Information, Figure 6S). A typical sensorgram for **GNP-9** can be seen in Fig. 2. A one site binding model was applied in the BIA evaluation software (Uppsala, Sweden) as this best represents

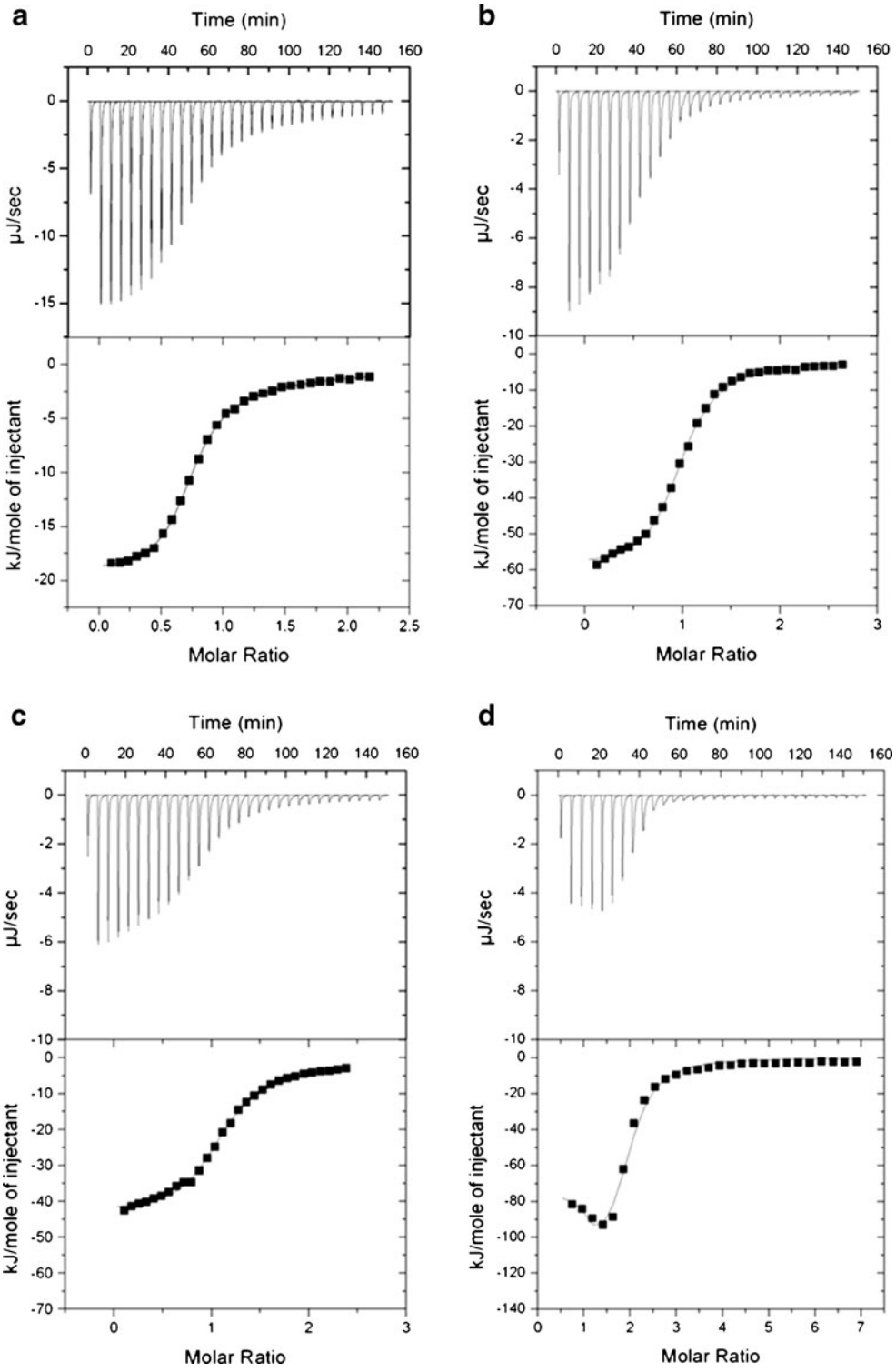

Fig. 3 ITC profiles for (**a**) the "standard" titration of BC2L-A ([BC2L-A_{dimer}]=0.15 mM in the cell) by injections of **3** ([3]= 3 mM in the syringe). The molar ratio here refers to the number of mannoside monomers per BC2L-A dimer. **b–d** "Reverse" titrations of the GNPs (in the cell) by BC2L-A (in the syringe). Molar ratios here refer to the number of BC2L-A dimers per mannoside ligand. **b** the titration of **GNP-7** ([3]=0.088 mM in the cell) by BC2L-A ([BC2L-Adim]= 0.52 mM in the syringe), **c** the titration of **GNP-8** ([3]= 0.09 mM in the cell) by BC2L-A ([BC2L-Adim]=0.5 mM in the syringe) and **d** the titration of **GNP-9** ([**3**]=0.013 mM in the cell) by BC2L-A ([BC2L-Adim]=0.2 mM in the syringe). Concentrations of the mannoside, **3**, are given as (monovalent) thiol concentrations. All experiments were carried out at 25 °C. *Solid black squares* represent the data points, the *black lines* represent the theoretical fits

the macroscopic absorption and desorption of the GNPs from the BC2L-A functionalised surface as measured by SPR. The association (k_a) and dissociation (k_d) rate constants, as well as the calculated association (K_a) and dissociation (K_d) constants, are shown in Table 2. **GNP-1** – **GNP-6**, displaying glucose and galactose on their surface, showed no binding to the BC2L-A channel. The *galactose*-GNPs showed strong binding to the PA-IL surface whilst glucose- and *mannose*-GNPs did not (data not shown). None of the GNPs tested showed binding to ethanolamine.

From Table 2 it can be seen that from a 13 % mannose presentation density (**GNP-7**) to 25 % (**GNP-8**) there is already an increase in ligand activity of over 10 fold. However, increasing the mannose presentation density to 46 % (**GNP-9**) induces a significant amplification of ligand activity with an 800 fold increase for **GNP-9** compared with **GNP-8**, and over 10 000 fold compared with **GNP-7**. Upon further increasing mannose presentation density to 100 % (**GNP-10**), ligand activity returns to a level comparable to **GNP-8**. The increase in *Ka* from **GNP-7**, **-8** and **-10** implies that GNP valency has a positive influence on mannose avidity towards BC2L-A. This suggests that effective concentrations induce a subtle cluster glycoside effect between these binding partners. However, this is much less significant than observed for other lectin systems such as PA-IL [21]. This is most likely due to the fact that BC2L-A is a dimer and therefore the possible binding permutations are significantly limited compared to a lectin with higher valence, despite the cooperative nature of BC2L-A [40]. The most important observation of the multivalence effect is the case of **GNP-9**, which is clearly due to a significant decrease in the macroscopic dissociation rate. This has been observed previously and related to a decrease in entropic penalties of the ligand leaving the binding site [32]. However, the decrease in *kd* may also be due to structural complementarities between **GNP-9** and lectin architecture. If the inter-ligand distance at **GNP-9** permitted bivalent binding to the surface bound lectin dimer, where lower presentation densities did not, the observed macroscopic GNP dissociation from the chip surface would be significantly reduced; due to thermodynamically having to break a bivalent lectin-GNP interaction as opposed to a monovalent interaction for other GNPs, as well as statistical rebinding effects.

Isothermal titration calorimetry

Further investigation of the thermodynamics of BC2L-A–GNP binding was carried out using isothermal titration microcalorimetry (ITC). SPR studies demonstrated that presenting mannose ligands on a GNP platform induced significant affinity improvements for BC2L-A binding. Due to the therapeutic importance of BC2L-A and related lectins, as well as a need to assess the functional properties of GNP scaffolded ligands, ITC was used to further

Table 3 Microcalorimetry of **3** and **GNP-7** – **9** binding to BC2L-A using the cooperative two-site model

	K_{a1} (10^6 M^{-1})	K_{d1} (μM)	ΔG_1 (kJ mol^{-1})	ΔH_1 (kJ mol^{-1})	$-T\Delta S_1$ (kJ mol^{-1})	β_1	K_{a2} (10^6 M^{-1})	K_{d2} (μM)	ΔG_2 (kJ mol^{-1})	ΔH_2 (kJ mol^{-1})	$-T\Delta S_2$ (kJ mol^{-1})	β_2
3	(1.8±0.4)	0.56	(−35.7±5)	(−19.0±3)	(−16.7±2)		(0.06±0.01)	14.8	(−27.6±5)	(−19.2±3)	(−8.4±2)	
GNP-7	(0.16±0.02)	6.5	(−29.5±0.3)	(−36.0±1)	(6.5±1.4)	0.1	(0.27±0.07)	4.1	(−30.9±0.7)	(−25.7±1.9)	(−5.2±1.2)	4.5
GNP-8	(1.0±0.1)	1.0	(−34.4±0.1)	(−27.3±0.5)	(−7.1±0.6)	0.6	(0.14±0.01)	7.1	(−29.3±0.1)	(−15.9±0.1)	(−13.4±0.1)	2.3
GNP-9	(52±19)	0.019	(−47±1)	(−73±19)	(26±18)	29	(1.7±0.2)	0.59	(−33.8±0.3)	(6.5±9.8)	(−40±10)	25

Errors are the standard deviations over 2 or 3 experiments. β is the potency of binding with reference to molecule **3**

characterise mannose presentation on GNP surfaces and their interaction with BC2L-A. The thermograms and titration curves can be seen in Fig. 3. Strong exothermic responses can be seen from the ITC profiles due to the binding between BC2L-A and the mannose ligands. Despite the titrations of ligand **3**, **GNP-7** and **GNP-8** exhibiting what resemble classical sigmoid curves, the fitting of the one-site model was not satisfactory due to the cooperative nature of the lectin. Therefore, a two-site model was fitted to the 5 data, which had been used previously for interactions of this lectin [24]. Lectin concentrations are therefore expressed as BC2LA dimers. The concentration of nanoparticles was expressed as a concentration of mannose residues, confirmed by the phenolsulfuric acid method used previously [21]. Molar ratios are defined as the ratio of [injectant]/[macromolecule in cell]. *Ka, Kd* and thermodynamic binding parameters for mannoside **3** (thiol form) and GNPs tested are listed in Table 3 and shown in Fig. 4. It was found that **GNP-10**, which has a 100 % mannose coverage, was not soluble in sufficient quantities in the buffer solution hence no ITC data is given. Injections of buffer into GNP solutions resulted in negligible heats of dilution. Injections of BC2L-A into solutions of galactose (80 %)/glucose (20 %)-functionalised **GNP-4** (see Supporting Information, Figure 7S) served as a reference for lectin dilution, which was subtracted from the *mannose*-GNP thermograms.

The dissociation constants and thermodynamic contributions measured for **3** are comparable to those observed for mannose monosaccharide derivatives (*Kd1*=2.7 μM, *Kd2*= 7.8 μM for Me-α- D-mannoside) [24]. However, for the second binding event, a reduction in favourable enthalpic contributions is offset by an increase in favourable entropic contributions when compared to Me-α-D-mannoside. Although **3** is depicted as a thiol (monovalent) in solution it also exists as a disulfide (divalent). However, ^{1}H NMR prior to ITC experiments did not show the presence of the

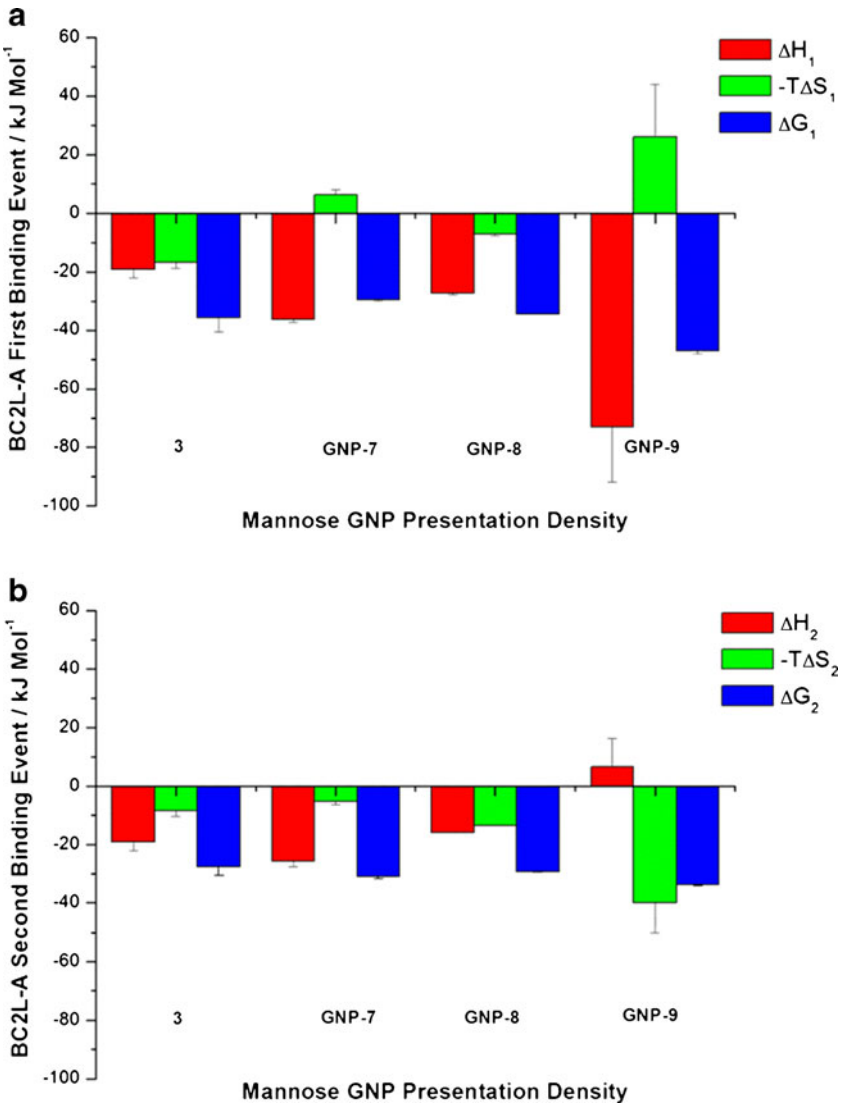

Fig. 4 Graphs of ITC results for BC2L-A (two-site model): Thermodynamic parameters of the first (**a**) and second (**b**) binding events. ΔG, *blue*; ΔH, *red* and (-TΔS) *green*

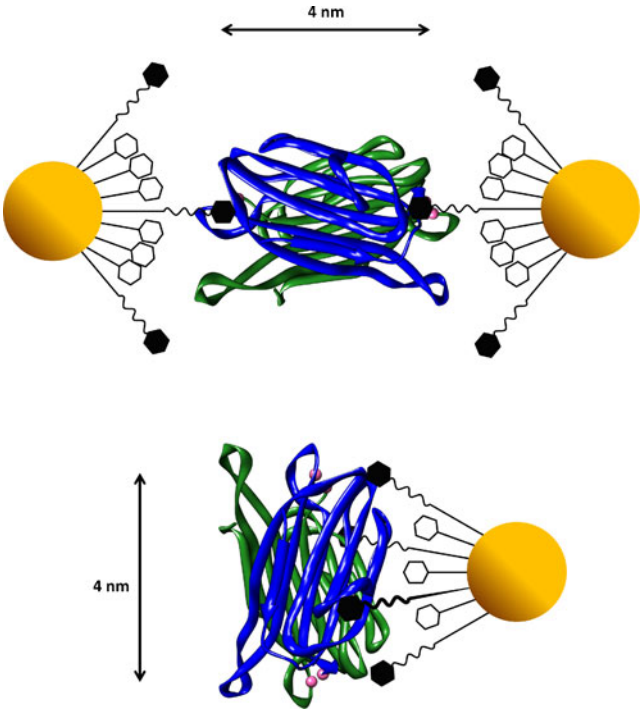

Fig. 5 Schematic representation of BC2L-A interacting with mannose functionalised GNPs. Above, intermolecular binding to BC2L-A by ligands from two GNPs of low presentation density. Below, bidentate intramolecular binding to BC2L-A by ligands on the same GNP presented in high density. *Solid hexagons* represent active mannose ligands, *hollow hexagons* represent inactive glucose ligands. Diagrams are not to scale

disulfide. Furthermore, experimental data indicate that had the divalent system formed during the experiment, it did not significantly improve the binding affinity of the monovalent compound.

From the dissociation constants observed for the GNP systems, there appears to be little advantage for the ligands presented with a low density on a GNP surface. For the first binding event, a reduction in binding potency was observed for GNP-7 and GNP-8, with binding potency factors, β_1, of 0.1 and 0.6 respectively (where $\beta_1 = K_{d1,3}/K_{d1},GNP$) [5]. The reduction in binding potency for these GNPs is related to a significant decrease in favourable entropic contributions, despite the increase in favourable enthalpic contributions. For the second binding event, a binding potency factor, β_2, of 4.5 and 2.3 was observed for GNP-7 and GNP-8, respectively. This is due to a similar enthalpic enhancement for the ligands present on the GNP surface, yet the entropic penalties experienced are reduced compared with the first binding event.

For **GNP-9** however, with a higher presentation density on the GNP surface, a four-fold enthalpic enhancement is observed, resulting in a K_{d1} of 19 nM and binding potency factor of 29 for the first binding event, despite increased entropic penalties. For the second binding event, a K_{d2} of 588 nM and a binding potency factor of 25 was observed, which is due to favourable entropic contributions despite small unfavourable enthalpic penalties. This means that for both binding events, mannose ligands presented on **GNP-9** are almost 30 times more active compared to the mannose ligand in free solution.

Relating ligand presentation to binding kinetics and thermodynamics

The results from SPR and ITC suggest that a GNP presentation density greater than 25 %, or an inter-ligand distance (Table 1) less than 2.4 nm, is required in order to significantly increase ligand avidity. Despite that (GNP inter-ligand distance) < (lectin inter-binding site distance) even for low density presentations, and that bivalent GNP–lectin interactions would be possible, the bivalent complex may incur enthalpic and entropic penalties in order for the ligands to adopt the correct conformation to interact with the lectin's second binding site [6]. Therefore, low density presentations may nevertheless favour the formation of a second intermolecular interaction (GNP-lectin-GNP complex, Fig. 5, upper part), which could also lead to aggregate structures [41].

As the inter-ligand distance at the GNP surface approaches half of the inter-binding site distance of the lectin dimer (4 nm as measured from the crystal structure [24]) the probability of a favourable second intra-molecular interaction will be increased (Fig. 5, lower part). This will lock the binding partners in a bidentate interaction and would explain the kinetics observed by SPR, with the multivalence effect experienced by **GNP-9** principally due to a significant reduction in dissociation rate constant, *kd*. The bidentate binding mode would also prevent a second GNP binding to the lectin, therefore no further translational or rotational degrees of freedom would be lost. Moreover, favourable entropic contributions would be observed with the displacement of ordered water, not only from the binding sites, but also from the solvent-accessible surface areas (of both the lectin and the GNP) *between* the binding sites. Despite this, there may nevertheless be a degree of structural mismatching between ligand conformation at **GNP-9** and the binding sites of the receptor. This would result in an enthalpic penalty, the magnitude of which being dependent on the rigidity of the linker molecules and the scaffold itself [6]. Therefore, it would be possible to have a multivalent interaction which may be entropically favoured, but enthalpically disfavoured as seen for **GNP-9**. Similar thermodynamic properties were observed by De *et al.* for the interactions of proteins with amino acid functionalised gold nanoparticles [42]. From an effective concentration point of view, an inter-ligand distance matching the inter-binding site distance would allow the possibility of a multivalent intramolecular interaction. However, reducing the interligand distance further would increase the number of intramolecular binding permutations, thus a multivalent intramolecular interaction is more likely to occur. Reducing the

interligand distance further still would result in more intramolecular binding permutations, but ligand organisation, packing and accessibility at higher presentation densities on the AuNP surface may also induce further enthalpic and entropic consequences.

By studying the case of BC2L-A interactions with mannose functionalised GNPs, a combination of structural compatibilities and effective concentrations is most likely required to correctly describe the experimentally observed multivalence effects. However, due to the dimeric architecture of the lectin, structural complementarities are likely to have a greater importance compared to lectins with multimeric architectures, where statistical contributions and effective concentrations would have a greater influence [20, 21].

The results obtained by SPR and ITC are in agreement with each other. They show similar trends between GNP presentation density and ligand activity. However, SPR shows an increase in ligand activity for GNP-9 of over 2 000 fold, whereas ITC shows only a 30-fold increase for the same GNP. The reason for this is most certainly due to SPR measuring the binding event *via* heterogeneous binding and dissociation with the lectin immobilised to the chip surface, whereas ITC measures the same binding event in a homogenous, solution phase. Indeed, immobilising the lectin to the SPR chip surface simplifies the binding interaction under study by removing the possibility of complex binding intermediates (aggregate structures *etc.*) which would otherwise contribute to, and be observed in, homogenous, solution phase experiments such as ITC. However, compared to ligand binding in the lectin's natural state, immobilising the lectin to a surface may reduce the effects of translational and rotational entropy upon GNP binding compared to solution phase binding. Equally, these entropy effects may be exaggerated when in free solution.

Conclusion

In summary, gold nanoparticles have been used as a scaffold to present mannoside ligands at different presentation densities. A combination of analytical techniques and a mathematical model have been used for calculating the distance between mannose ligands at the GNP surface. The influence of ligand presentation on recognition by the mannose-specific lectin BC2L-A has been investigated quantitatively, using surface plasmon resonance and isothermal titration calorimetry techniques. We have shown that a mannose presentation density greater than 25 %, or an interligand distance less than 2.4 nm, is required in order to induce a significant cluster glycoside effect on BC2L-A recognition, with a 2 000 fold increase in ligand avidity as measured by SPR, and a K_d of 19 nM as measured by ITC, for a 46 % mannose presentation density (**GNP-9**); the most effective BC2L-A binding partner to date.

Due to the pathogenicity of *Burkholderia cepacia* infections, resistance to clinically useful antibiotics and their transmissibility between patients [43], we again demonstrate the potential for GNPs as potent anti-adhesives for the prevention of pathogen invasion [18, 40]. Furthermore the facile, tuneable synthesis of functionalised AuNP platforms allows them to be simultaneously tailored with several different ligands (including fluorescent markers, antigens *etc.*). This in turn allows for a flexible approach towards multifunctional inhibitors preventing lectin mediated invasion of *B. cenocepacia*. In concert with our efforts in the application of GNP technology as medical and diagnostic tools, further characterisation and investigation of their fundamental properties will allow for a fuller understanding and exploitation of the multivalence/cluster glycoside effect at the molecular level.

Acknowledgments The authors wish to thank the GlycoGold research training network, a part of the sixth research framework of the European Union, contract number MRTN-CT-2004-005645, for financial support. Financial support from the CNRS and ESRF are also acknowledged as well from the Labex Arcane (ANR-11-LABX-003) and the COST actions CM1102 and BM1003. We thank also the Spanish Ministry of Science and Innovation (MICINN, grant CTQ2011-27268) and the Department of Industry of the Basque Country (Etortek 2009). Dr Emilie Lameignere is greatly appreciated for help with lectin production. The SPR experiments were ran thanks to access to a Biacore T100 at the Plateforme Nanobio-Grenoble. SAXS experiments and analysis were carried out with the help of Drs Michael Sztucki and Emanuela Di Cola (ESRF, Grenoble). Professors Monica Palcic and Johannis Kamerling are also thanked for their helpful discussion.

References

1. Lis, H., Sharon, N.: Lectins: carbohydrate-specific proteins that mediate cellular recognition. Chem. Rev. **98**, 637–674 (1998)
2. Varki, A., Cummings, R.D., Esko, J.D., Freeze, H.H., Stanley, P., Bertozzi, C.R., Hart, G.W., Etzler, M.E.: Essentials of Glycobiology, 2nd edn. Cold Spring Harbour, New York (2009)
3. Kramer, R.H., Karpen, J.W.: Spanning binding sites on allosteric proteins with polymer-linked ligand dimers. Nature **395**, 710–713 (1998)
4. Gargano, J.M., Ngo, T., Kim, J.Y., Acheson, D.W., Lees, W.J.: Multivalent inhibition of AB(5) toxins. J. Am. Chem. Soc. **123**, 12909–12910 (2001)
5. Mammen, M., Choi, S.K., Whitesides, G.M.: Polyvalent interactions in biological systems: Implications for design and use of multivalent ligands and inhibitors. Angew. Chem. Int. Ed. **37**, 2755–2794 (1998)
6. Reynolds, M., Perez, S.: Thermodynamics and chemical characterization of protein-carbohydrate interactions: the multivalency issue. C. R. Chim. **14**, 74–95 (2011)
7. Bernardi, A., Jimenez-Barbero, J., Casnati, A., De Castro, C., Darbre, T., Fieschi, F., Finne, J., Funken, H., Jaeger, K.E., Lahmann, M., Lindhorst, T.K., Marradi, M., Messner, P., Molinaro, A., Murphy, P.V., Nativi, C., Oscarson, S., Penadés, S., Peri, F., Pieters, R.J., Renaudet, O., Reymond, J.L., Richichi, B., Rojo, J., Sansone, F., Schaffer, C., Turnbull, W.B., Velasco-Torrijos, T., Vidal, S., Vincent, S., Wennekes, T., Zuilhof, H., Imberty, A.: Multivalent glycoconjugates as anti-pathogenic agents. Chem. Soc. Rev. (2013). doi:10.1039/C2CS35408J

8. Marradi, M., Chiodo, F., Garcia, I., Penadés, S.: Glyconanoparticles as multifunctional and multimodal carbohydrate systems. Chem. Soc. Rev. (2013). doi:10.1039/C2CS35420A
9. Tvaroska, I., Sihelnikova, L.: Step by step towards understanding gold glyconanoparticles as elements of the nanoworld. Chem. Pap. **61**, 237–255 (2007)
10. Marradi, M., Martin-Lomas, M., Penadés, S.: Glyconanoparticles polyvalent tools to study carbohydrate-based interactions. Adv. Carbohyd. Chem. Biochem. **64**, 211–290 (2010)
11. Boisselier, E., Astruc, D.: Gold nanoparticles in nanomedicine: preparations, imaging, diagnostics, therapies and toxicity. Chem. Soc. Rev. **38**, 1759–1782 (2009)
12. Otsuka, H., Akiyama, Y., Nagasaki, Y., Kataoka, K.: Quantitative and reversible lectin-induced association of gold nanoparticles modified with alpha-lactosyl-omega-mercapto-poly(ethylene glycol). J. Am. Chem. Soc. **123**, 8226–8230 (2001)
13. Lin, C.C., Yeh, Y.C., Yang, C.Y., Chen, C.L., Chen, G.F., Chen, C.C., Wu, Y.C.: Selective binding of mannose-encapsulated gold nanoparticles to type 1 pili in *Escherichia coli*. J. Am. Chem. Soc. **124**, 3508–3509 (2002)
14. Thygesen, M.B., Sauer, J., Jensen, K.J.: Chemoselective capture of glycans for analysis on gold nanoparticles: carbohydrate oxime tautomers provide functional recognition by proteins. Chem. Eur. J. **15**, 1649–1660 (2009)
15. Halkes, K.M., de Souza, A.C., Maljaars, C.E.P., Gerwig, G.J., Kamerling, J.P.: A facile method for the preparation of gold glyconanoparticles from free oligosaccharides and their applicability in carbohydrate-protein interaction studies. Eur. J. Org. Chem. 3650–3659 (2005).
16. Schofield, C.L., Mukhopadhyay, B., Hardy, S.M., McDonnell, M.B., Field, R.A., Russell, D.A.: Colorimetric detection of *Ricinus communis* Agglutinin 120 using optimally presented carbohydrate-stabilised gold nanoparticles. Analyst **133**, 626–634 (2008)
17. Martinez-Avila, O., Hijazi, K., Marradi, M., Clavel, C., Campion, C., Kelly, C., Penadés, S.: Gold manno-glyconanoparticles: multivalent systems to block HIV-1 gp120 binding to the lectin DC-SIGN. Chem. Eur. J. **15**, 9874–9888 (2009)
18. Martinez-Avila, O., Bedoya, L.M., Marradi, M., Clavel, C., Alcami, J., Penadés, S.: Multivalent manno-glyconanoparticles inhibit DC-SIGN-mediated HIV-1 trans-infection of human T cells. Chem Bio Chem **10**, 1806–1809 (2009)
19. Marradi, M., Di Gianvincenzo, P., Enriquez-Navas, P.M., Martinez-Avila, O.M., Chiodo, F., Yuste, E., Angulo, J., Penadés, S.: Gold nanoparticles coated with oligomannosides of HIV-1 glycoprotein gp120 mimic the carbohydrate epitope of antibody 2G12. J. Mol. Biol. **410**, 798–810 (2011)
20. Wang, X., Matei, E., Gronenborn, A.M., Ramstrom, O., Yan, M.: Direct measurement of glyconanoparticles and lectin interactions by isothermal titration calorimetry. Anal. Chem. **84**, 4248–4252 (2012)
21. Reynolds, M., Marradi, M., Imberty, A., Penades, S., Perez, S.: Multivalent gold glycoclusters: high affinity molecular recognition by bacterial lectin PA-IL. Chem. Eur. J. **18**, 4264–4273 (2012)
22. Govan, J.R., Deretic, V.: Microbial pathogenesis in cystic fibrosis: mucoid *Pseudomonas aeruginosa* and *Burkholderia cepacia*. Microbiol. Rev. **60**, 539–574 (1996)
23. Lyczak, J.B., Cannon, C.L., Pier, G.B.: Lung infections associated with cystic fibrosis. Clin. Microbiol. Rev. **15**, 194–222 (2002)
24. Lameignere, E., Malinovska, L., Slavikova, M., Duchaud, E., Mitchell, E.P., Varrot, A., Sedo, O., Imberty, A., Wimmerova, M.: Structural basis for mannose recognition by a lectin from opportunistic bacteria *Burkholderia cenocepacia*. Biochem. J. **411**, 307–318 (2008)
25. Sulak, O., Cioci, G., Delia, M., Lahmann, M., Varrot, A., Imberty, A., Wimmerova, M.: A TNF-like trimeric lectin domain from *Burkholderia cenocepacia* with specificity for fucosylated human histo-blood group antigens. Structure **18**, 59–72 (2010)
26. Sulak, O., Cioci, G., Lameignere, E., Balloy, V., Round, A., Gutsche, I., Malinovska, L., Chignard, M., Kosma, P., Aubert, D.F., Marolda, C.L., Valvano, M.A., Wimmerova, M., Imberty, A.: *Burkholderia cenocepacia* BC2L-C is a super lectin with dual specificity and proinflammatory activity. PLoS Pathog **7**, e1002238 (2011)
27. Lameignere, E., Shiao, T.C., Roy, R., Wimmerova, M., Dubreuil, F., Varrot, A., Imberty, A.: Structural basis of the affinity for oligomannosides and analogs displayed by BC2L-A, a *Burkholderia cenocepacia* soluble lectin. Glycobiology **20**, 87–98 (2010)
28. Mandal, D.K., Kishore, N., Brewer, C.F.: Thermodynamics of lectin-carbohydrate interactions. Titration microcalorimetry measurements of the binding of N-linked carbohydrates and ovalbumin to concanavalin A. Biochemistry **33**, 1149–1156 (1994)
29. Rieger, J., Stoffelbach, F., Cui, D., Imberty, A., Lameignere, E., Putaux, J.L., Jerome, R., Jerome, C., Auzely-Velty, R.: Mannosylated poly(ethylene oxide)-b-poly(epsilon-caprolactone) diblock copolymers: synthesis, characterization, and interaction with a bacterial lectin. Biomacromolecules **8**, 2717–2725 (2007)
30. Rieger, J., Freichels, H., Imberty, A., Putaux, J.L., Delair, T., Jerome, C., Auzely-Velty, R.: Polyester nanoparticles presenting mannose residues: toward the development of new vaccine delivery systems combining biodegradability and targeting properties. Biomacromolecules **10**, 651–657 (2009)
31. Sztucki, M., Narayanan, T.: Development of an ultra-small-angle X-ray scattering instrument for probing the microstructure and the dynamics of soft matter. J. Appl. Crystallogr. **40**, S459–S462 (2007)
32. Hostetler, M.J., Wingate, J.E., Zhong, C.-J., Harris, J.E., Vachet, R.W., Clark, M.R., Londono, J.D., Green, S.J., Stokes, J.J., Wignall, G.D., Glish, G.L., Porter, M.D., Evans, N.D., Murray, R.W.: Alkanethiolate gold cluster molecules with core diameters from 1.5 to 5.2 nm: core and monolayer properties as a function of core size. Langmuir **14**, 17–30 (1998)
33. Jadzinsky, P.D., Calero, G., Ackerson, C.J., Bushnell, D.A., Kornberg, R.D.: Structure of a thiol monolayer-protected gold nanoparticle at 1.1 A resolution. Science **318**, 430–433 (2007)
34. Huang, W., Bulusu, S., Pal, R., Zeng, X.C., Wang, L.S.: Structural transition of gold nanoclusters: from the golden cage to the golden pyramid. ACS Nano **3**, 1225–1230 (2009).
35. Chien, Y.Y., Jan, M.D., Adak, A.K., Tzeng, H.C., Lin, Y.P., Chen, Y.J., Wang, K.T., Chen, C.T., Chen, C.C., Lin, C.C.: Globotriose-functionalized gold nanoparticles as multivalent probes for Shiga-like toxin. Chem Bio Chem **9**, 1100–1109 (2008)
36. Kulkarni, A.A., Fuller, C., Korman, H., Weiss, A.A., Iyer, S.S.: Glycan encapsulated gold nanoparticles selectively inhibit shiga toxins 1 and 2. Bioconjugate Chem. **21**, 1486–1493 (2010)
37. Hill, H.D., Millstone, J.E., Banholzer, M.J., Mirkin, C.A.: The role radius of curvature plays in thiolated oligonucleotide loading on gold nanoparticles. ACS Nano **3**, 418–424 (2009)
38. Cederquist, K.B., Keating, C.D.: Curvature effects in DNA:Au nanoparticle conjugates. ACS Nano **3**, 256–260 (2009)
39. Schreiber, F.: Structure and growth of self-assembling monolayers. Prog. Surf. Sci. **65**, 151–256 (2000)
40. Rojo, J., Diaz, V., de la Fuente, J.M., Segura, I., Barrientos, A.G., Riese, H.H., Bernad, A., Penadés, S.: Gold glyconanoparticles as new tools in antiadhesive therapy. Chem Bio Chem **5**, 291–297 (2004)
41. Sisu, C., Baron, A.J., Branderhorst, H.M., Connell, S.D., Weijers, C.A., de Vries, R., Hayes, E.D., Pukin, A.V., Pieters, R.J., Zuihof, H., Visser, G.M., Turnbull, W.B.: The influence of ligand valency on aggregation mechanisms for inhibiting bacterial lectins.Chem Bio Chem. **10**, 329–337 (2009)
42. De, M., You, C.C., Srivasta, S., Rotello, V.M.: Biomimetic interactions of proteins with functionalized nanoparticles. J Am Chem Soc. **129**, 10747–10753 (2009)
43. Nzula, S., Vandamme, P., Govan, J.R.: Influence of taxonomic status on the in vitro antimicrobial susceptibility of the *Burkholderia cepacia* complex. J. Antimicrob. Chemother. **50**, 265–269 (2002)